analytical chemistry

Article

Cite This: *Anal. Chem.* 2019, 91, 3860−3868

pubs.acs.org/ac

Native Nano-electrospray Differential Mobility Analyzer (nES GEMMA) Enables Size Selection of Liposomal Nanocarriers Combined with Subsequent Direct Spectroscopic Analysis

Victor U. Weiss,*,† Karin Wieland,† Andreas Schwaighofer, Bernhard Lendl, and Guenter Allmaier

Institute of Chemical Technologies and Analytics, Vienna University of Technology (TU Wien), A-1060 Vienna, Austria

Supporting Information

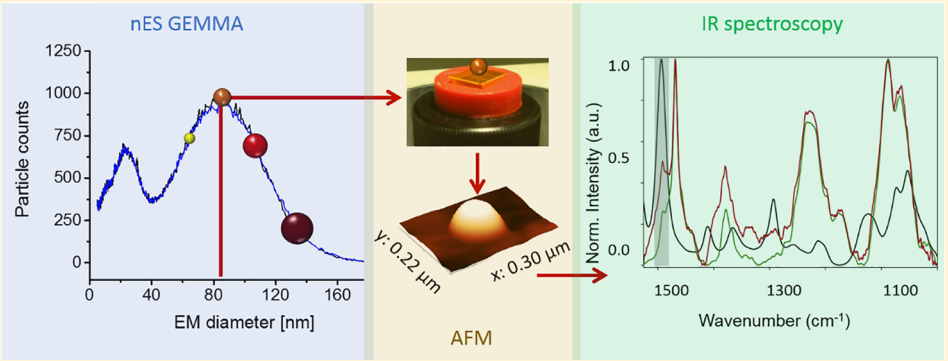

ABSTRACT: Gas-phase electrophoresis employing a nano-electrospray differential mobility analyzer (nES DMA), aka gas-phase electrophoretic mobility molecular analyzer (nES GEMMA), enables nanoparticle separation in the gas-phase according to their surface-dry diameter with number-based concentration detection. Moreover, particles in the nanometer size range can be collected after size selection on supporting materials. It has been shown by subsequent analyses employing orthogonal methods, for instance, microscopic or antibody-based techniques, that the surface integrity of collected analytes remains intact. Additionally, native nES GEMMA demonstrated its applicability for liposome characterization. Liposomes are nanometer-sized, biodegradable, and rather labile carriers (nanoobjects) consisting of a lipid bilayer encapsulating an aqueous lumen. In nutritional and pharmaceutical applications, these vesicles allow shielded, targeted transport and sustained release of bioactive cargo material. To date, cargo quantification is based on bulk measurements after bilayer rupture. In this context, we now compare capillary electrophoresis and spectroscopic characterization of vesicles in solution (bulk measurements) to the possibility of spectroscopic investigation of individual, size-separated/collected liposomes after nES GEMMA. Surface-dried, size-selected vesicles were collected intact on calcium fluoride (CaF_2) substrates and zinc selenide (ZnSe) prisms, respectively, for subsequent spectroscopic investigation. Our proof-of-principle study demonstrates that the off-line hyphenation of gas-phase electrophoresis and confocal Raman spectroscopy allows detection of isolated, nanometer-sized soft material/objects. Additionally, atomic force microscopy-infrared spectroscopy (AFM-IR) as an advanced spectroscopic system was employed to access molecule-specific information with nanoscale lateral resolution. The off-line hyphenation of nES GEMMA and AFM-IR is introduced to enable chemical imaging of single, i.e., individual, liposome particles.

Since its first appearance in literature,[1] gas-phase electrophoresis on a nES GEMMA (nano-electrospray gas-phase electrophoretic mobility molecular analysis) instrument has evolved to be a valuable tool for the characterization and analysis of a great variety of materials in the lower nanometer-size scale. nES GEMMA separates single-charged nanoparticles obtained from a nES process with subsequent charge equilibration. Analyte separation is based on the surface-dry nanoparticle size (electrophoretic mobility (EM) diameter) in a high laminar flow of dried air and a tunable electric field. By variation of the field strength, only particles of a certain EM diameter are capable to pass the size analyzer of the instrument toward a detector/collector. A corresponding setup (known as well as nES DMA, MacroIMS, ES SMPS, or LiquiScan ES) has been shown to provide information for, e.g., proteins,[2,3] viruses and virus-like particles,[4,5] nanoparticles,[6−9] exosomes,[10] and liposomes.[11−13] Besides the information on surface-dry nanoparticle size with number-based concentration particle detection in accordance with the recommendation of the European Commission for nanoparticle analysis (2011/696/EU from October 18, 2011), a correlation between the EM diameter and the nanoparticle molecular weight based on well-defined standard material can be established. This correlation enables the assessment of the molecular weight of an analyte

Received: September 18, 2018
Accepted: February 8, 2019
Published: February 8, 2019

DOI: 10.1021/acs.analchem.8b04252
Anal. Chem. 2019, 91, 3860−3868

based on its EM diameter as was shown by Bacher and colleagues for proteins in great detail in 2001.[2] In addition, even the molecular weight determination of larger proteinaceous complexes, for instance intact viruses, in a size and molecular weight range not easily accessible for classical mass spectrometric techniques[5] is possible. Conditions during the native nES process and gas-phase electrophoresis have recently been shown to be especially favorable for larger aggregates not even disrupting the noncovalent interactions between lectins and glycoproteins.[14]

In addition, nES GEMMA offers a size-selection step enabling the collection of nanoparticles of a defined size on flat surfaces for subsequent analysis via orthogonal methods. Electron microscopy of size-selected analytes was demonstrated, e.g., by Kallinger et al.[8] for silver nanoparticles and by Allmaier et al.[15] for tobacco mosaic virus. Likewise, atomic force microscopy (AFM) was successfully applied.[16] Furthermore, Havlik et al.[16] as well as Engel at al.[14] coupled nES GEMMA size separation off-line with dot blot analysis. Hence, it was demonstrated that nanoparticles remained identifiable for corresponding antibodies after gas-phase electrophoresis, proving that the surface structure of collected species was still intact after collection. Holder and Marr showed that silver nanoparticles can be directly sampled to cultured cells for subsequent cytotoxicity experiments.[17]

We now focus on the combination of nES GEMMA with spectroscopic techniques to gain additional, molecule-specific information on size-separated material in the nanometer-size range. Specifically, we use Raman and mid-infrared spectroscopy to perform chemical imaging of liposomes. In the methods, spectral features are evoked by molecular vibrations and can be assigned to specific functional groups. The spectrum represents the chemical fingerprint of the analyte, which is accessed in a direct, noninvasive way, providing information on chemical bonds as well as spatial arrangement and chemical interaction of molecules with the possibility of quantification.

Signal generation in Raman spectroscopy is based on an inelastic scattering process, i.e., the sample is illuminated with a short wavelength (VIS or NIR) light source and the light scattered off the sample contains additional wavelengths that are due to interaction with the sample. Given the short wavelength and using a confocal microscope, it should be possible to push the lateral resolution of Raman low enough to allow imaging of individual liposomes (here ∼100 nm).

In contrast, infrared spectroscopy is based on an absorption process performed at wavelengths between 400 and 4000 cm^{-1} (mid-IR). The spatial resolution achievable with far-field mid-IR spectroscopy is diffraction-limited at 2−5 μm.[18,19] To achieve spatial resolution on the single-liposome scale, we employ a near-field detection technique based on photothermal induced resonance in an AFM cantilever. In short, the sample placed in an AFM is illuminated by a pulsed tunable infrared laser. Absorption of infrared radiation leads to rapid, local expansion of the absorber, which is transduced as a damped oscillation by the AFM cantilever positioned above the sample. This technique—called AFM-IR or photothermal induced resonance (PTIR)—has been demonstrated to give similar infrared spectra as far-field infrared spectroscopy, but with spatial resolutions down to 20 nm.[18,20] Increased signal sensitivity can be achieved using resonance-enhanced AFM-IR. Here, the repetition rate of the laser is set according to the frequency of the contact resonance of the AFM cantilever, necessitating constant tracking thereof throughout the measurement.[20,21]

In our study we selected small unilamellar liposomes as model nanoparticle objects. These vesicles consist of a lipid bilayer encapsulating an aqueous volume. Hence, cargo compounds can be transported either in the lumen, the lipid bilayer, or the bilayer-associated layer according to the cargo hydrophobicity.[22] The cargo encapsulation efficiency of vesicles is usually assessed via chromatographic[23] or electrophoretic[24] assays. We employed capillary electrophoresis as well as spectroscopic bulk measurements prior to gas-phase electrophoresis to investigate cargo encapsulation. Subsequently, vesicles were size-separated/selected and collected on flat substrates to allow their microscopic and spectroscopic investigation. First, employing confocal Raman microscopy, we successfully demonstrated that Raman signals of liposomal structures collected on CaF_2 can be detected. However, facing limitations in signal sensitivity and lateral resolution (diffraction limit), in the second step, we opted for an advanced optical system to access chemical-specific information on individual liposomes beyond the diffraction limit. In our proof-of-principle study, we were able to show that AFM-IR is a promising method for destruction-free investigation of single, i.e., individual, nanocarriers, increasing the lateral resolution of obtained spectroscopic images. Our work indicates that off-line hyphenation of gas-phase electrophoresis and spectroscopy opens the avenue for thorough in-depth investigation of soft nanoparticle material in terms of size, shape, and chemical information. We believe that our method of off-line hyphenation will enable investigation of size-selected analytes from complex mixtures in the future, potentially resolving distributions of chemicals inside isolated nanocarriers.

MATERIALS AND METHODS

Additional detailed information on applied chemicals, liposome preparation, and instrumentation as well as sample preparation including AFM height maps of liposomes with different deposition methods can be found in the Supporting Information.

Liposome Preparation. In addition to liposomes similar to those employed in a previous study[12] (HSPC/Chol/DSPE-mPEG2000 in a 5.5:4.0:0.5 molar ratio, encapsulating a fluorophore at 10 μM concentration in 40 mM NH_4OAc, pH 8.4, from now on termed PEGylated liposomes), liposomes from HSPC/Chol/DSPE (5.7:3.8:0.5 molar ratio) were prepared according to the thin lipid film hydration technique.[25]

Instrumentation. Native nES GEMMA measurements were carried out on a TSI, Inc., instrument (Shoreview, MN, U.S.A.). It consists of a nES aerosol generator (model 3480) equipped with a ^{210}Po α-particle source, a nano differential mobility analyzer (nDMA) (model 3080) for separation, and a *n*-butanol-based ultrafine condensation particle counter (CPC) (model 3025A or model 3776C) for detection. A 25 μm inner diameter, fused silica capillary with a homemade tip[26] was used for generation of a stable Taylor cone. A fresh capillary was employed for each day of measurement to exclude cross-contamination. Liposomes were collected on calcium fluoride (CaF_2) or zinc selenide (ZnSe) prisms for subsequent AFM and spectroscopic imaging after particle passage through the nDMA and applying an electrostatic nanometer aerosol sampler (ENAS, model 3089, TSI, Inc.) at −3 to −3.1 kV

DOI: 10.1021/acs.analchem.8b04252
Anal. Chem. 2019, 91, 3860−3868

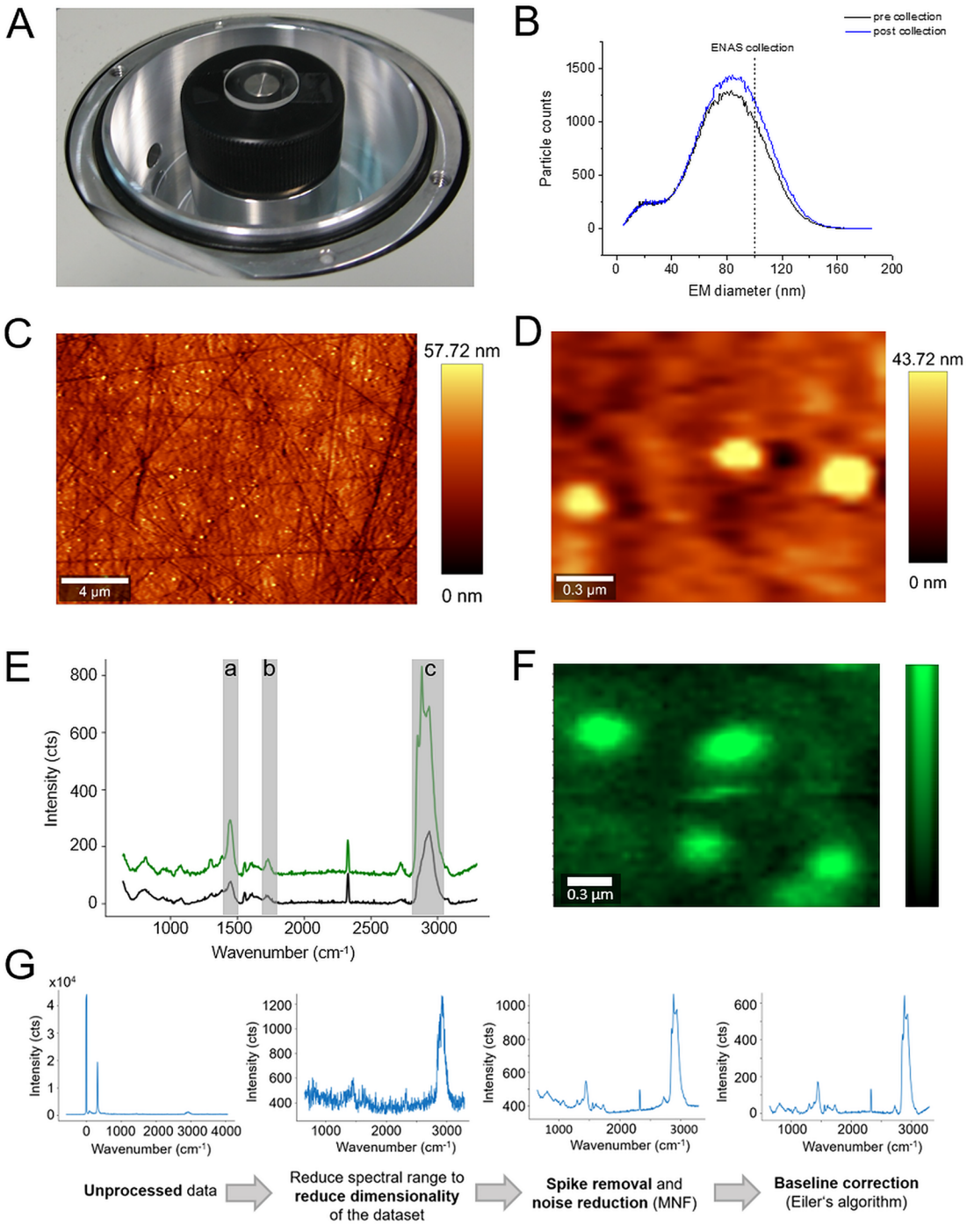

Figure 1. CaF_2 substrate was placed on top of the electrode in the ENAS unit of the nES GEMMA instrument (A) to size-select liposomes for Raman spectroscopy. After collection of intact liposomal nanocarriers at 100 nm EM diameter (B), the distribution of single vesicles was investigated via AFM height maps (C). The stability of the nES GEMMA instrument during particle collection is demonstrated by the very similar spectra measured prior to and after particle collection (B). A closer look at the AFM height map indicates elliptical structures on the substrate with a width between 200 and 250 nm and a height of 40−45 nm (D). Raman spectra collected on (green) and between (black) these elliptical structures show a similar spectral fingerprint but exhibit different signal intensity with the liposome signal (green) being significantly higher (E). The intensity distribution of the integrated CH stretching vibration (~2920 cm^{-1}) depicts similar structures as observed in the AFM height map; however, the elliptical structures in the Raman map are blurred and measure a width of 300−350 nm, indicating insufficient lateral resolution (F). Data processing scheme (G).

and 1.5 L per minute (Lpm) air flow for 120 min at 85 nm EM diameter.

A custom-made, 3D-printed holder was designed for stable ZnSe prism montage in the ENAS. Polylactic acid (PLA)-based fused deposition modeling (FDM) was employed using a self-built 3D printer with a nozzle diameter of 0.4 mm. Capillary electrophoresis was performed with an Agilent 3D CE instrument (Agilent Technologies, Waldbronn, Germany) employing 200 mM sodium borate, pH 8.4, as background electrolyte (BGE).

DOI: 10.1021/acs.analchem.8b04252
Anal. Chem. 2019, 91, 3860−3868

Nonencapsulated material was removed from vesicles via spin filtration.[9] On the basis of the weighed initial liposome amount (of a 10 μL volume) and the weighed liposome material after buffer exchange, a 1:10 [v/v] dilution of the initial stock (i.e., final 1 mM lipid concentration in samples) was achieved.

AFM measurements in contact mode (WITec AFM Arrow Cantilever reflex-coated: 0.2 N/m, 14 kHz) were performed of liposomes with and without encapsulated drug deposited on either ZnSe or CaF_2 substrates using a WITec alpha 300 RSA+ confocal microscope (Ulm, Germany). The microscope was equipped with a 20× magnification objective (Zeiss EC Epiplan, NA 0.4, Zeiss, Jena, Germany) and an internal cantilever drive mount. Project FIVE (WITec) and Gwyddion 2.44 software were used for subsequent data analysis.

A WITec alpha 300 RSA+ confocal Raman microscope equipped with a 488 nm excitation laser (DPSS laser, <50 mW, laser class 3B) was used for Raman imaging of liposomes. The laser was focused onto the sample through a 100× objective (Zeiss, NA 0.9). Backscattered photons were collected in reflection mode with the same objective, resulting in a lateral resolution of 220 nm based on the diffraction limit for confocal microscopes. The Stokes signal (anti-Stokes and Rayleigh light is removed via an edge filter) is detected with a fiber coupled spectrometer (UHTS 300 spectrometer VIS, f/4 300 mm focal length) equipped with a 600 grooves/mm grating (blaze wavelength = 500 nm) and a highly sensitive, thermoelectrically cooled electron-multiplying charged-coupled device (EMCCD) camera allowing a spectral resolution of 2−3 cm^{-1}. After nES GEMMA separation/collection on flat CaF_2 substrates (Raman grade, Crystran, Poole, U.K.), the sample was fixed on a piezo-stage on top of a motorized sample stage enabling a lateral positioning accuracy of <2 nm. Balancing signal intensity and thermal stress exerted onto the sample, Raman images were collected with a laser power of 43 mW and 1 s of integration time covering an area of 10 × 10 μm^2 with 50 nm step size in x- and y-direction. Control FOUR (WITec) software was used for data acquisition.

Raman images were processed (see Figure 1G) using ImageLab (Epina, Pressbaum, Austria). First, the data matrix was reduced by selecting the spectral range between 650 and 3290 cm^{-1} for each spectrum/pixel to reduce the dimensionality of the data cube and speed up calculation time for subsequent processing steps. After spike removal, maximum noise fraction (MNF, noise structure: horizontal stripes) was performed to reduce noise in the spectra. As a last step, the spectra were baseline-corrected using Eiler's algorithm (λ = 10^5, p = 0.0020, 7 iterations).[27]

AFM-IR measurements were performed using a NanoIR 1 system (Anasys Instruments, Santa Barbara, CA, U.S.A.) operated in bottom-up illumination equipped with a pulsed tunable IR source (MIRcat, Daylight Solutions, San Diego, CA, U.S.A.) covering the spectral range from 789 to 1763 cm^{-1}.

AFM-IR spectra were processed using Solo+MIA software (Eigenvector Research, Inc., Manson, WA, U.S.A., release 8.1.1). To increase the signal-to-noise ratio, Savitzky Golay smoothing (window size: 11, zeroth order polynomial) was applied before cutting the data set selecting the spectral range between 1200 and 1770 cm^{-1}. For better comparison, baseline-corrected spectra (Automatic Whittaker Filter: λ = 1000, p = 0.000001) were scaled between 0 and 1.

RESULTS AND DISCUSSION

Within the last few years, gas-phase electrophoresis on a native nES GEMMA instrument evolved as a valuable analysis method for the characterization of nanoparticle material. Especially the collection of size-selected material for subsequent analysis employing orthogonal methods enables in-depth nanoparticle characterization. Here, we focus on spectroscopic techniques to gain additional, molecule-specific information on size-separated material in the lower nanometer-size range (i.e., below 100 nm surface-dry EM particle diameter).

Native nES GEMMA Collection of Size-Selected Liposomes Followed by Their Raman Spectroscopic Investigation. Following our findings in 2016,[12,13] we investigated the collection of size-selected PEGylated liposomal vesicles on supporting materials suitable for subsequent spectroscopic analysis. The simplest approach for deposition of particles from suspensions on substrates would be dropping the sample solution onto the substrate and letting it dry in an unforced way at room temperature. This approach, however, does not allow homogeneous particle distribution on the substrate. Furthermore, fragile particles such as liposomes have the tendency to burst during the drying process (see Figure S1 of the Supporting Information). nES GEMMA, besides yielding information on the analyte size distribution and the particle number concentration, allows collection of particles from suspension in a dry and intact form and offers additional features such as a customizable particle distribution density on the substrate and a size-selection step. For initial AFM and Raman measurements, we opted for vesicles similar in lipid composition and cargo material to those originally analyzed via nES GEMMA. Infrared microscopy with a lateral resolution of roughly 5 μm[18,19] is not applicable to spatially resolve individual PEGylated liposomes, which are in the size range of roughly 200 nm once collected on a substrate (see below). Therefore, because the diffraction limit is directly proportional to the wavelength of the emitting light source, we opted for confocal Raman spectroscopy/imaging. Corresponding laser sources emit light in the visible region with a lateral resolution of 220 nm for a confocal system with 488 nm laser excitation wavelength and 100× magnification (NA = 0.9). CaF_2 was used as supporting material (Figure 1A) because it exhibits a flat baseline in the spectral region of interest.[28,29] Native nES GEMMA spectra were collected prior to and post sample collection to check for stability of the system (Figure 1B). Prior to spectroscopic analysis, AFM images of PEGylated liposomes on CaF_2 with a sampling diameter of 100 nm (EM diameter) were recorded (i) to investigate the spatial distribution of the PEGylated liposomes on the substrate and (ii) to check if PEGylated liposomes were collected in an intact form on the substrate. Once PEGylated liposomes are collected on the substrate, their original spherical shape in solution changes to an ellipsoid one upon contact with the solid sample support. A width of ∼200−250 nm and a height in the range of 25−35 nm (Figure 1C and D) as detected via AFM lead to a particle volume of collected vesicles similar to values obtained for liposomes in the gas/liquid phase. Besides vesicle/substrate interaction, this deformation also results from the force exerted by the AFM tip. Investigation by Raman spectroscopy of the particles successfully revealed typical bands evoked by lipids such as the CH stretching vibration at ∼2920 cm^{-1}, the C═O stretching vibration at 1740 cm^{-1}, or the CH_2

DOI: 10.1021/acs.analchem.8b04252
Anal. Chem. 2019, 91, 3860−3868

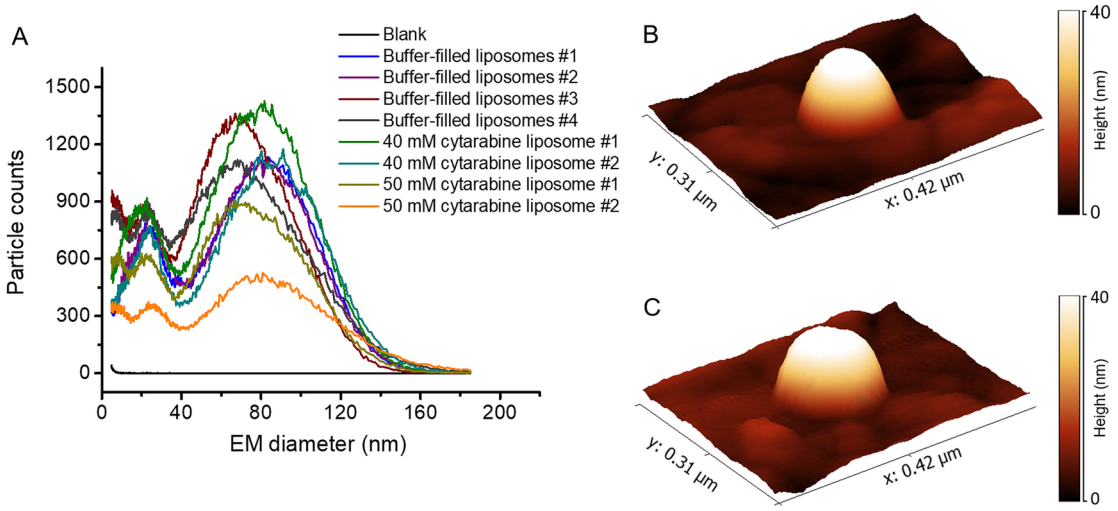

Figure 2. Native nES GEMMA data (A) of buffer-filled as well as cytarabine-encapsulating liposomes. No significant difference between these two vesicle types is detectable. This finding was also corroborated by AFM results in contact mode of buffer-filled liposomes (B) as well as vesicles encapsulating cytarabine cargo (C, preparation of vesicles in 40 mM cytarabine solution).

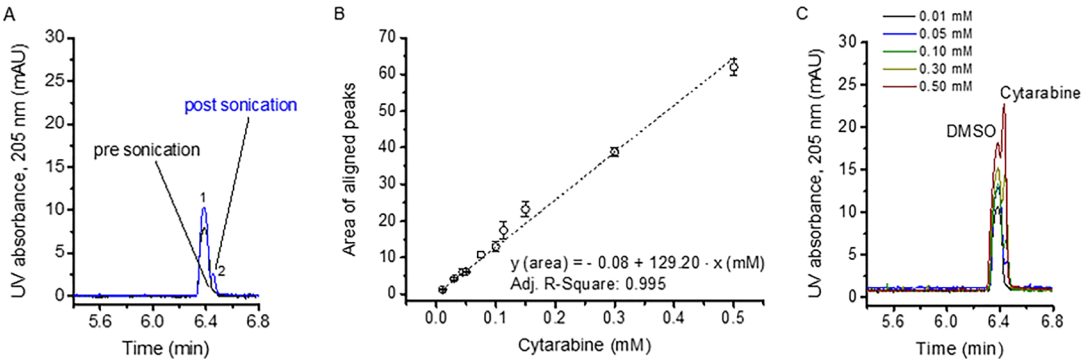

Figure 3. Amount of cytarabine encapsulated in vesicles being released upon liposome sonication (A) was determined via correlation of the analyte concentration and the obtained peak area (B) by measurement of cytarabine standards (C). CE with UV absorption detection at 205 nm was employed. Peak 1 corresponds to dimethylsulfoxide (DMSO) employed as internal standard, and peak 2 corresponds to cytarabine.

deformation vibration at 1440 cm^{-1}.[30] The intensity distribution of the integrated CH stretching vibration (2821 to 3056 cm^{-1}) as the most intense band in the Raman spectrum (Figure 1E) indicates that ellipsoid structures are indeed detected based on their lipid-specific spectral fingerprint. However, (i) the structures seem blurred and measure 300−350 nm in width, which is significantly broader than in AFM images of the same sample. Hence, while we successfully verify via AFM that only single liposomes are present on the substrate, chemical differences within a single liposome cannot be measured spectroscopically due to the diffraction limit of confocal Raman spectroscopy. Also, (ii) a very similar spectral fingerprint—although with significantly lower intensity—could be recorded from areas between PEGylated liposomes (black spectrum in Figure 1E). These two observations are most likely attributed to insufficient lateral resolution of the employed spectroscopic method. Furthermore, (iii) the original spectra of PEGylated liposomes before the processing steps show poor signal-to-noise ratios in the range of 2−6 (Figure 1G). (iv) We used CaF_2 as substrate for Raman spectroscopy, even though the surface of the substrate is rough, making it less suitable for AFM investigations. Considering that we ultimately want to develop a method that allows detection of the encapsulated cargo at even lower concentration compared to the lipid vesicles, Raman spectroscopy appears not to offer this possibility in terms of signal sensitivity and lateral resolution at the moment. Hence, we assessed the applicability of another spectroscopic method for our purpose and at the same time adapted the liposome system from our initial study[12,13] to a vesicle system encapsulating a chemotherapeutic drug.

Preparation and Characterization of Drug-Loaded Liposomes. For investigation of liposomes encapsulating a pharmacologically active compound, we opted for cytarabine—also known as cytosine arabinoside (ara-C) or 1β-arabinofuranosylcytosine. Cytarabine, employed, e.g., for leukemia treatment, was FDA approved already in April 1999. Only recently, a novel combination of cytarabine and daunorubicin in liposomes has been reported for treatment of acute myeloid leukemia with a corresponding pharmacological investigation published in 2018.[31]

After preparation, liposomes were analyzed via gas-phase electrophoresis on a nES GEMMA instrument according to an already established protocol.[12,13] Our analysis yielded liposome preparations with vesicles of 78.4 ± 6.5 nm surface-dry particle diameter at the peak apex and an average full peak width of 66.9 ± 7.3 nm at half peak height (Figure 2A). Note that filling of liposomes with cytarabine cargo had no impact on the vesicle appearance upon nES GEMMA analysis—vesicles were

DOI: 10.1021/acs.analchem.8b04252
Anal. Chem. 2019, 91, 3860−3868

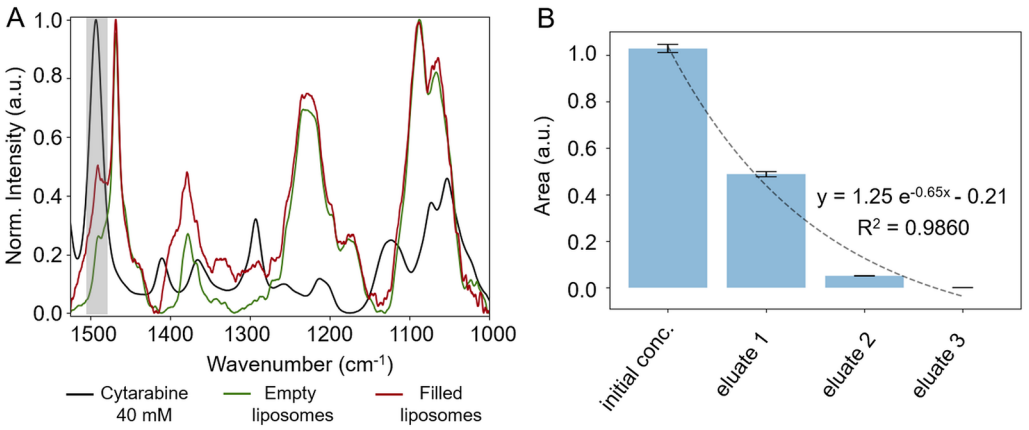

Figure 4. FTIR spectra of liposomes in plain buffer or encapsulating cytarabine measured in a transmission flow cell after exchange of nonencapsulated buffer material. For comparison, the FTIR spectrum of 40 mM cytarabine is shown. Cytarabine can be detected at 1494 cm^{-1} (highlighted in gray) besides signals originating from lipids (A). Removal of nonencapsulated cytarabine during spin-filtration can be followed by FTIR measurements (B).

prepared in the absence as well as in the presence of 40 and 50 mM cytarabine, respectively. Likewise, AFM data corroborates this finding (Figure 2B and C). Despite differences in obtained nanoparticle height and width values and their respective standard deviations (probably due to interactions of the AFM tip with soft matter analytes, i.e., liposomes, especially for vesicles not filled with corresponding cargo molecules), similar values for vesicle dimensions were obtained: buffer-filled liposomes (Figure 2B) were 160 ± 59 nm in width and 36 ± 15 nm in height (n = 20 individual particles), whereas vesicles encapsulating cytarabine (Figure 2C) were 158 ± 26 nm in width and 26 ± 10 nm in height (n = 21 individual particles).

It is of note that, in order to remove nonencapsulated cytarabine from individual preparations, vesicles were subjected to spin filtration.[9] Despite this purification step, still some low EM diameter material was detectable for our preparations; this material previously was assigned to unspecific aggregates of material employed during the vesicle-formation process, possibly lipid micelles or similar.[12,13] However, in relation to the main vesicle peak at 78.4 ± 6.5 nm EM diameter, the amount of this smaller-sized material seemed negligible for the experiments presented in this work (note, however, that the low EM diameter material had been shown to influence cell viability in a previous study).[12]

Applying capillary electrophoresis (CE) to such preparations after desalting allowed us to subsequently assess the amount of the encapsulated drug within vesicles similar to studies found in the literature.[32,33] CE of cytarabine-containing vesicles after desalting did not yield a peak for cytarabine (Figure 3A). Only after sonication, which had already been shown to disrupt vesicles and to release the vesicle cargo as seen due to the increase of smaller-sized sample components,[13] significant amounts of the employed drug were detectable (Figure 3A). Comparing the obtained peak area to the correlation between peak areas and sample concentrations of cytarabine standards with known analyte concentration (Figure 3B, at least n = 2 measurements per data point) analyzed via CE (Figure 3C) allows calculation of the analyte concentration within vesicles based on the following simplifications and assumptions: (i) 80 nm surface-dry liposome particle diameter as found approximately upon native nES GEMMA analysis of a corresponding sample (Figure 1), (ii) 10 mM overall lipid concentration based on the lipid amount employed in the vesicle-preparation process, (iii) the molar lipid ratio, and (iv) a phospholipid headgroup projected area of ∼0.7 nm^2 for phosphatidylcholine (PC),[34] 0.6 nm^2 for phosphatidylethanolamine (PE),[35] and 0.4 nm^2 for cholesterol.[36] Combining these numbers, a liposome concentration of ∼40 nM was determined. Taking into account this value as well as the volume of corresponding spheres based on approximation of the surface-dry particle diameter, a total liposome volume of ∼6 mL/L solution was obtained. Relating the liposome volume to the increase of analyte concentration upon vesicle sonication (∼0.04 mM) yielded the concentration of cytarabine inside vesicles (∼5 mM for various liposome preparations).

In a next step, we performed bulk Fourier transform infrared (FTIR) measurements of liposomes encapsulating cargo molecules. Employing a flow cell setup for transmission FTIR measurements, we successfully identified a characteristic band (evoked by C═C and C═N stretch vibrations[37]) for the detection of cytarabine in solution at 1494 cm^{-1} (Figure 4A). This characteristic band even allowed us to follow the removal of nonencapsulated cytarabine via spin-filtration by measurement of solutions that had passed the spin-filter membrane (Figure 4B). From the first to the second spin-filtration step (eluate 1 vs eluate 2), a significant reduction in cytarabine content of the eluate is demonstrated, indicating that most of the nonencapsulated cytarabine is removed in the first spin filtration step. Nevertheless, a second washing step is necessary because cytarabine can still be detected by transmission FTIR spectroscopy after the second spin-filtration step, whereas no cytarabine was detectable after the third spin-filtration (eluate 3), proving successful removal of nonencapsulated cytarabine. This also means that any cytarabine signal detectable with FTIR spectroscopy of liposomes after spin-filtration is most certainly evoked by cytarabine vibrations inside the nanocarrier. Furthermore, as depicted by the small band at 1494 cm^{-1} in Figure 4A, besides IR bands that can be related to lipid building blocks, cytarabine is detectable in samples containing vesicle-encapsulated cargo after spin-filtration. After calculating the difference spectrum of filled and empty liposomes, the concentration of encapsulated cytarabine can be estimated based on the area ratio of the characteristic cytarabine band in the difference spectrum and the FTIR spectrum of 40 mM cytarabine. Hence, a cytarabine concentration of roughly 1

DOI: 10.1021/acs.analchem.8b04252
Anal. Chem. 2019, 91, 3860−3868

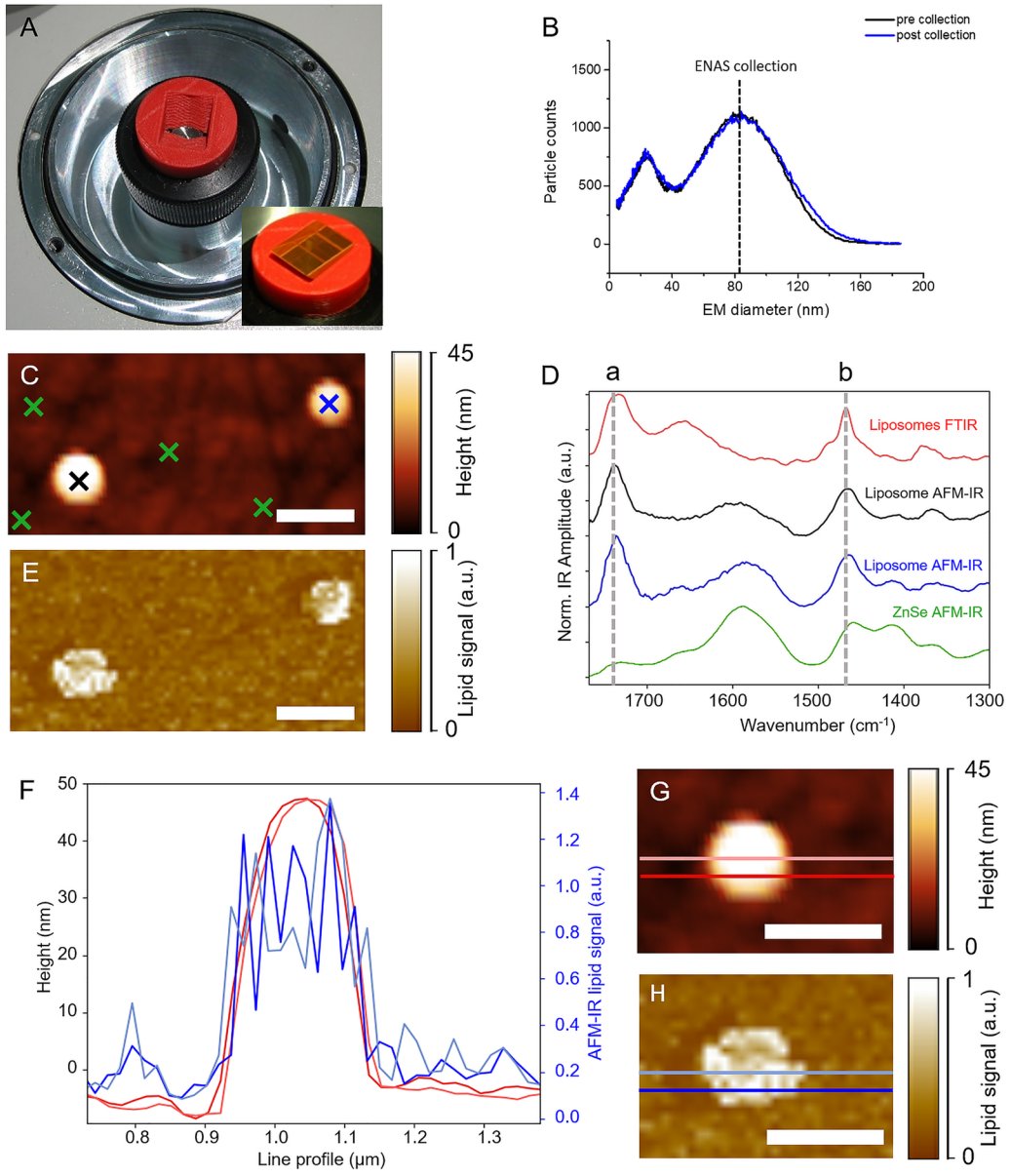

Figure 5. AFM-IR spectroscopy of individual, size-selected liposomes collected on ZnSe prisms. Application of a 3D-printed support enabled positioning of prisms in the nES GEMMA ENAS unit (A). Liposomes were size-collected at 85 nm EM diameter from a liposome batch with heterogeneous size distribution. No significant differences in obtained spectra prior to and after size collection were detected (B). Single liposomes were selected based on the AFM height map depicting structures with a width of ∼150 nm and a height of 45−50 nm (C). AFM-IR spectra of individual liposomes with buffer as encapsulated cargo collected on positions indicated by color-coded crosses (e.g., blue cross in (C) corresponds to blue spectrum in (D)) in (C) are in good agreement with far-field FTIR-ATR spectra (red) of the same sample system. Typical vibrational bands such as (a) the carbonyl band at 1735 cm^{-1} or (b) the CH_2 deformation vibration at 1467 cm^{-1} evoked by lipids are marked by the dashed gray line. Spectra are normalized and offset for clarity (D). Tuning the laser to the carbonyl band (1735 cm^{-1}) results in a map depicting the spatial distribution of lipids with 17.5 nm step size in *x*- and *y*-direction (E). The lipid signal was referenced to the SiO_2 cantilever signal for reasons of better visualization. Line profiles (F) taken from the height map of a single liposome (G) compared to the lipid signal of the same liposome (H) outline that AFM-IR imaging provides sufficient lateral resolution to resolve a single liposome. The scale bar is 250 nm.

mM was determined that is in good agreement with the results obtained by CE measurements (roughly 5 mM). However, like CE, the application of this spectroscopic setup only allows bulk measurements; hence, only a calculated average drug concentration per liposomal vesicle can be obtained.

To conclude, gas-phase electrophoretic analysis for collection of size-selected cytarabine-filled vesicles in an intact form was demonstrated. The size and shape of isolated liposomes were investigated by AFM measurements. CE measurements confirmed that liposomes encapsulating cytarabine were successfully prepared, which was additionally verified by FTIR measurements. However, all these methods yielded information on the carrier itself or bulk analysis of the chemotherapeutic drug in general—no information on encapsulation efficiency and the cargo content of individual nanocarriers was obtainable.

Spectroscopic Investigation of Single Liposomal Nanocarriers. On the basis of our Raman spectroscopy results, we wanted to improve our method in terms of lateral resolution, signal sensitivity, and AFM image quality. In doing

DOI: 10.1021/acs.analchem.8b04252
Anal. Chem. 2019, 91, 3860−3868

so, we opted for resonance-enhanced AFM-IR spectroscopy promising a lateral resolution of 20 nm and a signal sensitivity that allows monolayer detection.[38,39]

In terms of substrate, we opted for ZnSe prisms as supporting material due to their good spectroscopic characteristics as well as surface smoothness necessary for AFM analysis. A ZnSe prism support was 3D-printed, allowing for prisms to be placed into the nES GEMMA ENAS unit. The 3D-printed support was fixed in the ENAS unit via double-sided tape, and the ZnSe prism was placed in the printed cavity without any additional support. An opening in the bottom of the 3D-printed support allowed contact between the electrode of the ENAS unit and the ZnSe prisms (Figure 5A).

Liposomes filled with buffer were collected at 85 nm EM diameter on ZnSe substrates. To check for stability of the nES GEMMA system, spectra prior to and post sampling were recorded and compared (Figure 5B). No significant differences between these two spectra could be observed, indicating a stable collection of particles over time.

Following ENAS collection, AFM analysis of collected vesicles was performed. After microscopic determination of the position of a vesicle on the ZnSe surface (Figure 5C), AFM-IR spectra were collected of individual liposomes with a collection diameter of roughly 100 nm (Figure 5D). Comparison of the near-field IR spectra with far-field FTIR-ATR spectra of the identical liposomal drug-delivery system shows that the spectra correspond well with each other. Both methods show characteristic bands evoked by molecule-specific vibrations of lipids such as the carbonyl band at 1735 cm^{-1} or the CH_2 deformation vibration at 1467 cm^{-1} wavenumbers.[40,41] Additionally, AFM-IR spectra of the ZnSe substrate were collected on different positions between single liposomes (Figure 5D). The average spectrum of four different measurement positions is depicted in Figure 5D and—compared to the AFM-IR spectra of single liposomes—does not exhibit any characteristic lipid bands. The AFM-IR map of the lipid signal (Figure 5E and H) indicates a similar shape as the height map of the same liposome (Figure 5C and G). For better visualization, the lipid AFM-IR signal was referenced to an internal standard (SiO_2 signal of the cantilever recorded at 1260 cm^{-1}). To demonstrate the lateral resolution that can be achieved with AFM-IR imaging, profile lines of the height image and the lipid map of the same liposome were compared (Figure 5F), highlighting the ability of AFM-IR to spatially resolve an individual, single liposome. Both maps show sharp features at the edge of the liposome and indicate the same liposome width of roughly 200 nm.

Identical collection and analysis steps were repeated for liposomes filled with cytarabine. However, so far, we have not been able to identify the encapsulated cargo based on the AFM-IR signal. This might be improved using a different geometric arrangement in the sample-light interaction. In the setup used in this work, the IR laser is focused onto the sample via bottom illumination. A higher AFM-IR signal intensity is to be expected using the top illumination arrangement, which would allow increased signal intensity due to the possibility of plasmonic enhancement using gold-coated tips and substrates. We concentrate on this setup in another study.[42]

To conclude, we were able to collect the spectral fingerprint of size-selected single liposomes employing AFM-IR spectroscopy. Nevertheless, despite our advance in lateral resolution upon switching from Raman to AFM-IR spectroscopy, we were still not able to extract spectroscopic information on the encapsulated cargo material inside liposomal vesicles.

CONCLUSIONS

With the current work we focus on the collection of liposomes after size-separation on a nES GEMMA instrument on a suitable analyte support for subsequent spectroscopic characterization. Prior to gas-phase electrophoresis, deployed liposomes were characterized via CE, AFM, and FTIR spectroscopy, especially concerning their encapsulated cargo in bulk measurements. Going one step further, we intended to access similar information but from individual nanocarriers. For this purpose, collection of size-selected, individual liposomal vesicles followed by spectroscopy-based identification of single nanocarriers was shown based on the application of our native nES GEMMA/spectroscopy off-line hyphenation.

Using Raman spectroscopy, we are able to demonstrate spectroscopy of individual liposomes. While the lateral resolution of confocal Raman microscopy per se is not sufficient to resolve individual liposomes, AFM microscopy can be used to ensure that only individual liposomes are evaluated. The combination of native nES GEMMA with AFM-IR spectroscopy is shown to give access to chemical information on single, nanosized vesicles. For both techniques, further improvements can be envisioned, such as using surface-enhanced Raman effects to improve the confocal Raman signal or using plasmonic enhancement in top illumination for AFM-IR.[38]

To conclude, native nES GEMMA/AFM-IR spectroscopy off-line hyphenation has been demonstrated to be a promising approach for label-free, nondestructive investigation of nanocarriers with sufficient nanoscale lateral resolution. We believe that, especially for drug as well as other bioactive ingredient-delivery nanoparticles in pharmaceutical, cosmetic, and food applications or naturally occurring material, e.g., exosomes, the noninvasive characterization of material via spectroscopic methods will yield valuable additional information on analytes.

ASSOCIATED CONTENT

Supporting Information

The Supporting Information is available free of charge on the ACS Publications website at DOI: 10.1021/acs.analchem.8b04252.

Chemicals, liposome preparation, native nES GEMMA measurements, CE measurements, buffer exchange of samples, instrumentation, and AFM height maps (PDF)

AUTHOR INFORMATION

Corresponding Author

*E-mail: victor.weiss@tuwien.ac.at. Tel.: +43 1 58801 151611. Fax: +43 1 58801 16199.

ORCID

Victor U. Weiss: 0000-0002-0056-6819

Andreas Schwaighofer: 0000-0003-2714-7056

Author Contributions

†V.U.W. and K.W. contributed equally to the manuscript. Initial idea: V.U.W., G.A., B.L.; liposome preparation, nES GEMMA, and CE measurements: V.U.W.; spectroscopic and AFM measurements: K.W., A.S.; instrumentation: G.A., B.L.; funding: B.L., G.A., V.U.W.; guidance: G.A., B.L.; all authors contributed to the manuscript.

DOI: 10.1021/acs.analchem.8b04252
Anal. Chem. 2019, 91, 3860−3868

Notes

The authors declare no competing financial interest.

■ ACKNOWLEDGMENTS

This project was supported by the Austrian Science Fund (FWF), Grant P25749-B20 (to V.U.W.). K.W. and A.S. acknowledge financial support by the Austrian research funding association (FFG) within the research project "NanoSpec−High-resolution near-field infrared microscopy for the process control of nanotechnological components" (Contract no. 843594). The authors thank Andrea Centrone and Georg Ramer (Center for Nanoscale Science and Technology, National Institute of Standards and Technology, Gaithersburg, Maryland, U.S.A.) for enabling AFM-IR measurements.

■ REFERENCES

(1) Kaufman, S. L.; Skogen, J. W.; Dorman, F. D.; Zarrin, F.; Lewis, K. C. *Anal. Chem.* **1996**, *68* (11), 1895−904.
(2) Bacher, G.; Szymanski, W. W.; Kaufman, S. L.; Zollner, P.; Blaas, D.; Allmaier, G. *J. Mass Spectrom.* **2001**, *36* (9), 1038−52.
(3) de la Mora, J. F.; Ude, S.; Thomson, B. A. *Biotechnol. J.* **2006**, *1* (9), 988−97.
(4) Kaddis, C. S.; Lomeli, S. H.; Yin, S.; Berhane, B.; Apostol, M. I.; Kickhoefer, V. A.; Rome, L. H.; Loo, J. A. *J. Am. Soc. Mass Spectrom.* **2007**, *18* (7), 1206−16.
(5) Weiss, V. U.; Bereszczak, J. Z.; Havlik, M.; Kallinger, P.; Gosler, I.; Kumar, M.; Blaas, D.; Marchetti-Deschmann, M.; Heck, A. J.; Szymanski, W. W.; Allmaier, G. *Anal. Chem.* **2015**, *87* (17), 8709−17.
(6) Dudkiewicz, A.; Wagner, S.; Lehner, A.; Chaudhry, Q.; Pietravalle, S.; Tiede, K.; Boxall, A. B.; Allmaier, G.; Tiede, D.; Grombe, R.; von der Kammer, F.; Hofmann, T.; Molhave, K. *Analyst* **2015**, *140* (15), 5257−67.
(7) Hinterwirth, H.; Wiedmer, S. K.; Moilanen, M.; Lehner, A.; Allmaier, G.; Waitz, T.; Lindner, W.; Laemmerhofer, M. *J. Sep Sci.* **2013**, *36* (17), 2952−61.
(8) Kallinger, P.; Weiss, V. U.; Lehner, A.; Allmaier, G.; Szymanski, W. W. *Particuology* **2013**, *11* (1), 14−19.
(9) Weiss, V. U.; Lehner, A.; Kerul, L.; Grombe, R.; Kratzmeier, M.; Marchetti-Deschmann, M.; Allmaier, G. *Electrophoresis* **2013**, *34* (24), 3267−76.
(10) Chernyshev, V. S.; Rachamadugu, R.; Tseng, Y. H.; Belnap, D. M.; Jia, Y.; Branch, K. J.; Butterfield, A. E.; Pease, L. F., 3rd; Bernard, P. S.; Skliar, M. *Anal. Bioanal. Chem.* **2015**, *407* (12), 3285−301.
(11) Epstein, H.; Afergan, E.; Moise, T.; Richter, Y.; Rudich, Y.; Golomb, G. *Biomaterials* **2006**, *27* (4), 651−9.
(12) Urey, C.; Weiss, V. U.; Gondikas, A.; von der Kammer, F.; Hofmann, T.; Marchetti-Deschmann, M.; Allmaier, G.; Marko-Varga, G.; Andersson, R. *Int. J. Pharm.* **2016**, *513* (1−2), 309−318.
(13) Weiss, V. U.; Urey, C.; Gondikas, A.; Golesne, M.; Friedbacher, G.; von der Kammer, F.; Hofmann, T.; Andersson, R.; Marko-Varga, G.; Marchetti-Deschmann, M.; Allmaier, G. *Analyst* **2016**, *141* (21), 6042−6050.
(14) Engel, N. Y.; Weiss, V. U.; Marchetti-Deschmann, M.; Allmaier, G. *J. Am. Soc. Mass Spectrom.* **2017**, *28* (1), 77−86.
(15) Allmaier, G.; Laschober, C.; Szymanski, W. W. *J. Am. Soc. Mass Spectrom.* **2008**, *19* (8), 1062−8.
(16) Havlik, M.; Marchetti-Deschmann, M.; Friedbacher, G.; Winkler, W.; Messner, P.; Perez-Burgos, L.; Tauer, C.; Allmaier, G. *Anal. Chem.* **2015**, *87* (17), 8657−64.
(17) Holder, A. L.; Marr, L. C. *BioMed Res. Int.* **2013**, *2013*, 328934.
(18) Dazzi, A.; Prater, C. B.; Hu, Q.; Chase, D. B.; Rabolt, J. F.; Marcott, C. *Appl. Spectrosc.* **2012**, *66* (12), 1365−84.
(19) Nasse, M. J.; Walsh, M. J.; Mattson, E. C.; Reininger, R.; Kajdacsy-Balla, A.; Macias, V.; Bhargava, R.; Hirschmugl, C. J. *Nat. Methods* **2011**, *8* (5), 413−416.
(20) Centrone, A. *Annu. Rev. Anal. Chem.* **2015**, *8*, 101−26.
(21) Ramer, G.; Reisenbauer, F.; Steindl, B.; Tomischko, W.; Lendl, B. *Appl. Spectrosc.* **2017**, *71* (8), 2013−2020.
(22) Gomez-Hens, A.; Fernandez-Romero, J. M. *TrAC, Trends Anal. Chem.* **2005**, *24* (1), 9−19.
(23) Xuan, T.; Zhang, J. A.; Ahmad, I. *J. Pharm. Biomed. Anal.* **2006**, *41* (2), 582−8.
(24) Franzen, U.; Nguyen, T. T.; Vermehren, C.; Gammelgaard, B.; Ostergaard, J. *J. Pharm. Biomed. Anal.* **2011**, *55* (1), 16−22.
(25) Bangham, A. D.; Standish, M. M.; Watkins, J. C. *J. Mol. Biol.* **1965**, *13* (1), 238−52.
(26) Tycova, A.; Prikryl, J.; Foret, F. *Electrophoresis* **2016**, *37* (7−8), 924−30.
(27) Eilers, P. H. C.; Boelens, H. F. M. *Baseline Correction with Asymmetric Least Squares Smoothing*; **2005**.
(28) Wieland, K.; Kuligowski, J.; Ehgartner, D.; Ramer, G.; Koch, C.; Ofner, J.; Herwig, C.; Lendl, B. *Appl. Spectrosc.* **2017**, *71* (12), 2661−2669.
(29) Schuster, K. C.; Reese, I.; Urlaub, E.; Gapes, J. R.; Lendl, B. *Anal. Chem.* **2000**, *72* (22), 5529−34.
(30) Huang, W. E.; Li, M.; Jarvis, R. M.; Goodacre, R.; Banwart, S. A. *Adv. Appl. Microbiol.* **2010**, *70*, 153−86.
(31) Nikanjam, M.; Capparelli, E. V.; Lancet, J. E.; Louie, A.; Schiller, G. *Cancer Chemother. Pharmacol.* **2018**, *81* (1), 171−178.
(32) Chen, D.; Cole, D. L.; Srivatsa, G. S. *J. Pharm. Biomed. Anal.* **2000**, *22* (5), 791−801.
(33) Perjesi, P.; Kim, T.; Zharikova, A. D.; Li, X.; Ramesh, T.; Ramasubbu, J.; Prokai, L. *J. Pharm. Biomed. Anal.* **2003**, *31* (5), 929−35.
(34) Dickey, A.; Faller, R. *Biophys. J.* **2008**, *95* (6), 2636−46.
(35) Murzyn, K.; Rog, T.; Pasenkiewicz-Gierula, M. *Biophys. J.* **2005**, *88* (2), 1091−103.
(36) Edholm, O.; Nagle, J. F. *Biophys. J.* **2005**, *89* (3), 1827−32.
(37) El-Subbagh, H. I.; Al-Badr, A. A. Chapter 2—Cytarabine. In *Profiles of Drug Substances, Excipients and Related Methodology*; Brittain, H. G., Ed.; Academic Press: 2009; Vol. *34*, pp 37−113.
(38) Lu, F.; Jin, M. Z.; Belkin, M. A. *Nat. Photonics* **2014**, *8* (4), 307−312.
(39) Ramer, G.; Aksyuk, V. A.; Centrone, A. *Anal. Chem.* **2017**, *89* (24), 13524−13531.
(40) Lewis, R. N. A. H.; Mcelhaney, R. N.; Pohle, W.; Mantsch, H. H. *Biophys. J.* **1994**, *67* (6), 2367−2375.
(41) Movasaghi, Z.; Rehman, S.; ur Rehman, I. *Appl. Spectrosc. Rev.* **2008**, *43* (2), 134−179.
(42) Wieland, K.; Ramer, G.; Weiss, V. U.; Allmaier, G.; Lendl, B.; Centrone, A. *Nano Res.* **2019**, *12* (1), 197−203.

DOI: 10.1021/acs.analchem.8b04252
Anal. Chem. 2019, 91, 3860−3868